Supplemental material

Goel et al., https://doi.org/10.1083/jcb.201807165

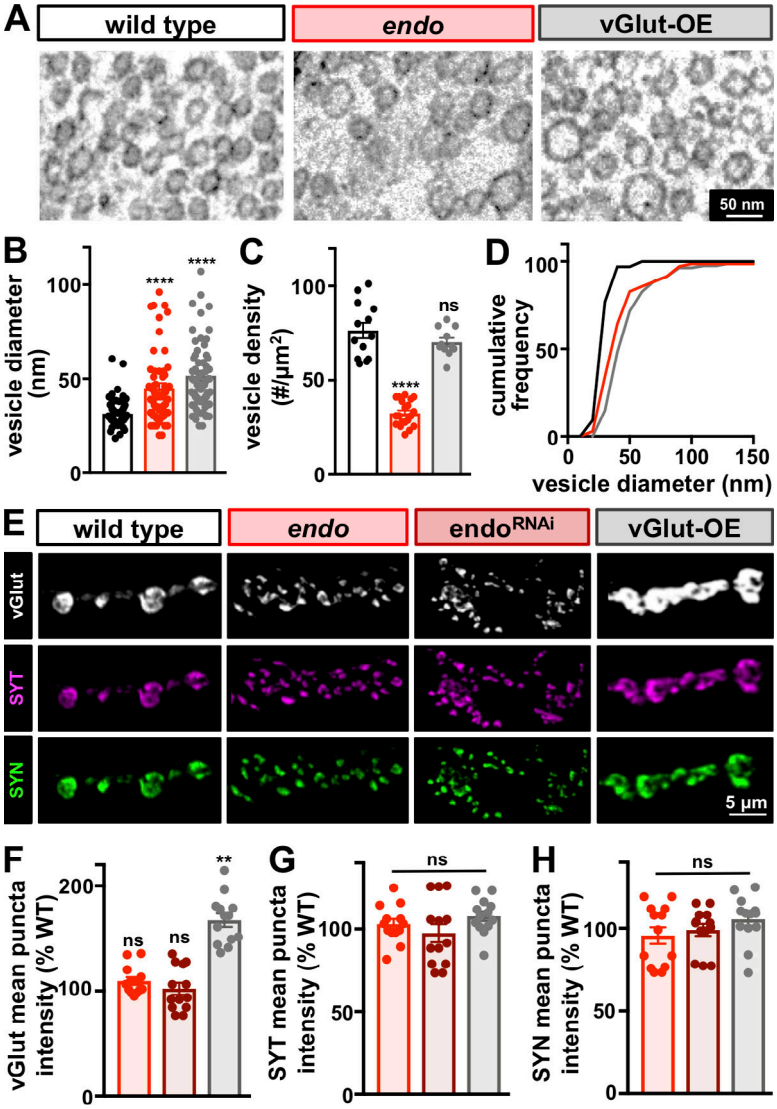

Figure S1. **Distinct mechanisms enlarge SVs and quantal size at *endo* and vGlut-OE synapses (related to Fig. 1). (A)** Representative electron micrographs of SVs at NMJ terminals from wild type, *endo*, and vGlut-OE. **(B)** Quantification of increased SV diameter in *endo* and vGlut-OE, consistent with increased glutamate emitted from these vesicles. **(C)** Quantification of SV density reveals a significant reduction in *endo* but no change in vGlut-OE compared with wild type ($n \geq 65$; one-way ANOVA, K-S test in D; Table S1). **(D)** Cumulative frequency distribution of SV diameter shows a rightward shift of the entire population in *endo* and vGlut-OE. **(E)** Representative images of individual boutons in the indicated genotypes immunostained with antibodies that recognize the SV markers vGlut (vesicular glutamate transporter), SYN (Synapsin), and SYT (Synaptotagmin). **(F–H)** Quantification of mean intensities of individual vGlut, SYN, and SYT puncta demonstrates a specific increase in vGlut intensity in vGlut-OE, as expected, with no change in puncta intensities of SYN or SYT. In contrast, intensity is unchanged in all SV markers in *endo* or endo^{RNAi}. Error bars indicate ± SEM ($n \geq 7$; one-way ANOVA; Table S1). **, $P < 0.01$; ****, $P < 0.0001$; ns, not significant.

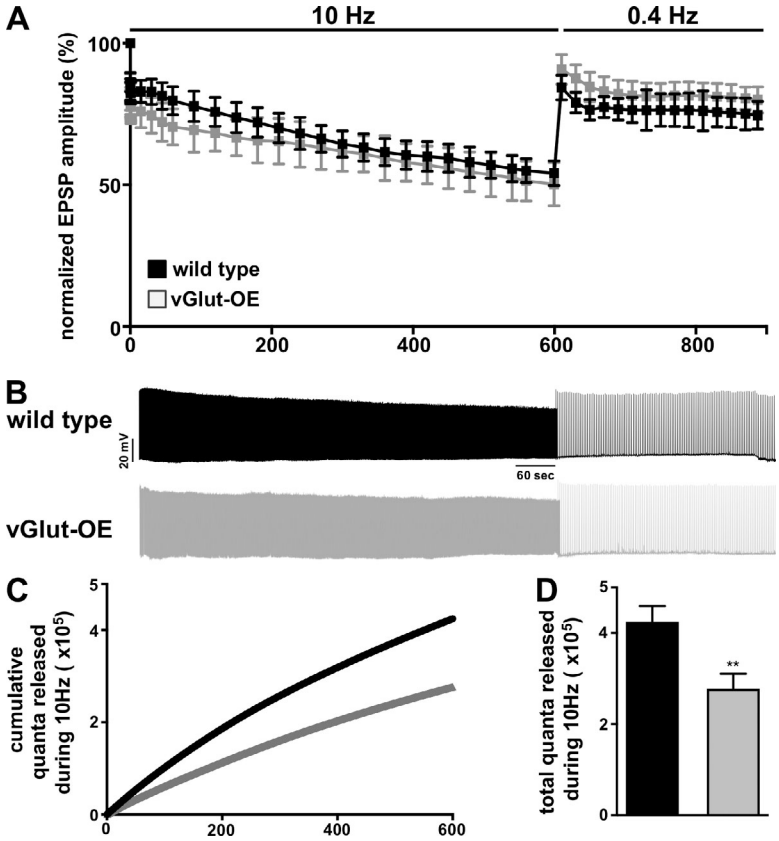

Figure S2. **SV recycling is unperturbed in vGlut-OE (related to Fig. 1). (A)** Wild-type and vGlut-OE NMJs were stimulated at 10 Hz for 10 min in 2 mM extracellular Ca^{2+} and subsequently allowed to recover with stimulation at 0.4 Hz. EPSP amplitudes were averaged (binning 2 s of responses for each time point), normalized to prestimulus amplitude, and plotted as a function of time. **(B)** Representative traces of experiments in A for the indicated genotypes. **(C)** Quantification of cumulative quanta released during the 10-min stimulation protocol in each genotype shows the expected reduction in vGlut-OE. **(D)** Quantification of the total quanta released in each genotype during the 10-Hz rundown period reveals a reduction in vGlut-OE. All error bars indicate ± SEM ($n \geq 7$; *t* test; Table S1). **, $P < 0.01$.

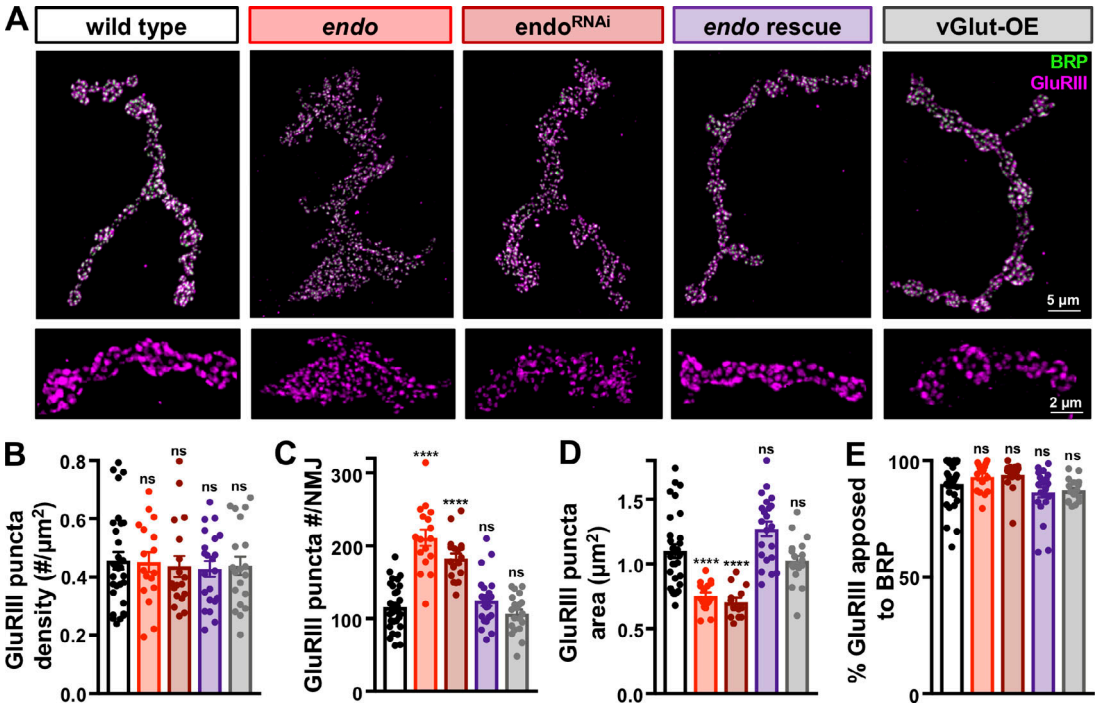

Figure S3. **Postsynaptic glutamate receptor fields mirror presynaptic AZ structure in *endo* mutants (related to Fig. 2). (A)** Representative NMJs in the indicated genotypes immunostained with antibodies against the essential postsynaptic glutamate receptor subunit GluRIII, with insets below representing individual boutons from the same NMJ. **(B)** No change in GluRIII density is observed in any genotype. **(C)** GluRIII puncta numbers per NMJ are significantly increased in *endo* and endo^{RNAi} and rescued in endo rescue, and no change is found in vGlut-OE. **(D)** A significant reduction in the area of individual GluRIII puncta is observed in *endo* and endo^{RNAi}, with no change in vGlut-OE. **(E)** No significant difference in the apposition of GluRIII puncta to BRP puncta is observed in any genotype. Error bars indicate ± SEM ($n \geq 12$; one-way ANOVA; Table S1). ****, $P < 0.0001$; ns, not significant.

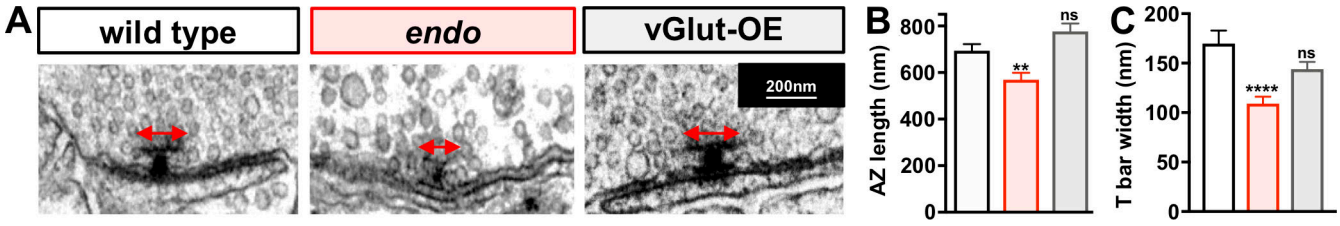

Figure S4. **Reduced AZ length and T-bar width in *endo* mutants revealed by EM (related to Figs. 2 and 5). (A)** Representative EM images of AZs in wild type, *endo* mutants, and vGlut-OE. The width of the T-bar structure at the center of the AZ in shown by the arrows. **(B and C)** Quantification of AZ length (B) and T bar width (C) in the indicated genotypes. All error bars indicate ± SEM ($n \geq 54$; one-way ANOVA; Table S1). **, $P < 0.01$; ****, $P < 0.0001$; ns, not significant.

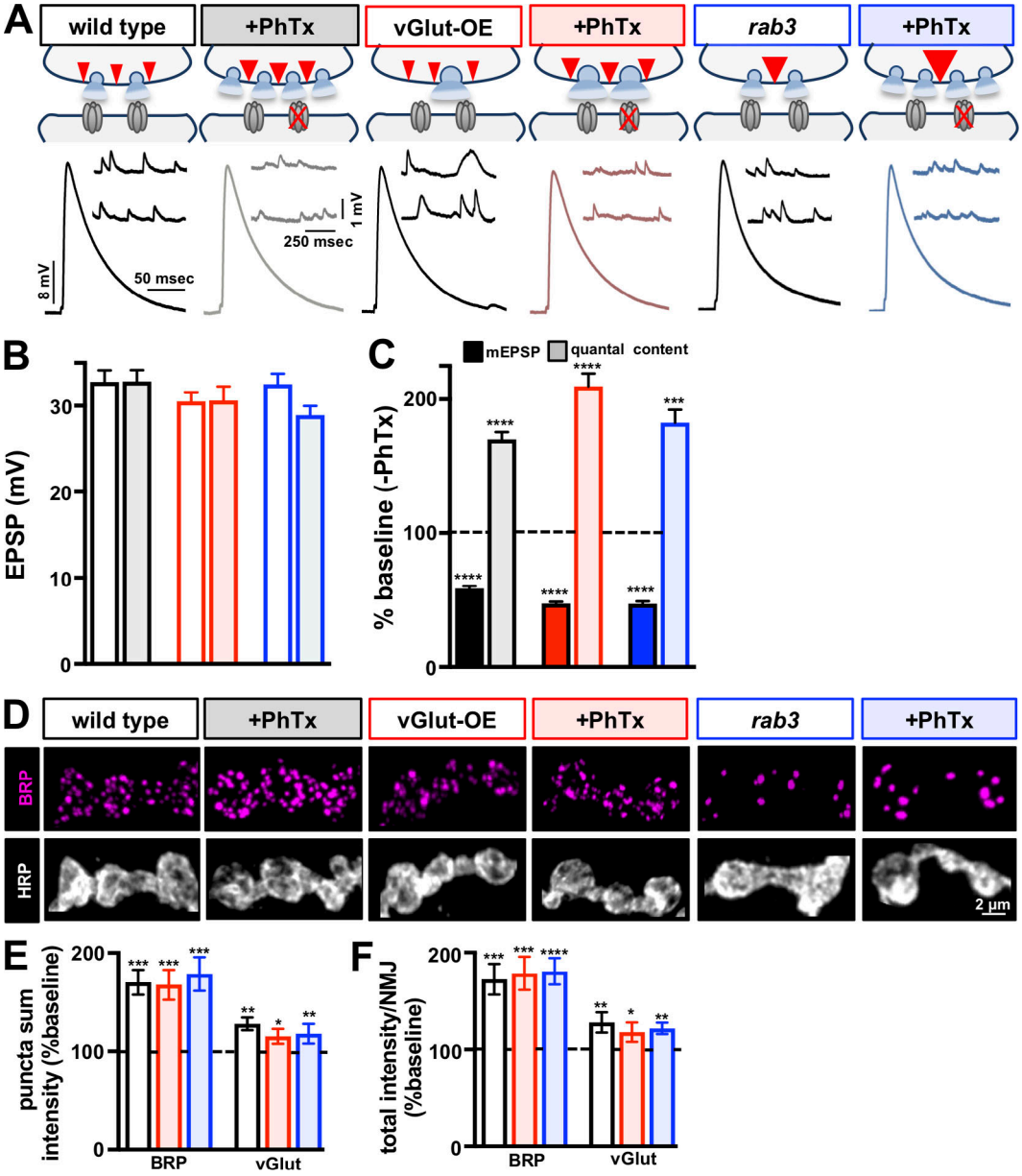

Figure S5. **NMJs expressing homeostatic depression or AZ scaling can acutely express homeostatic potentiation (related to Fig. 7). (A)** Schematic and representative traces of wild type, vGlut-OE, and *rab3* mutant NMJs before and after PhTx application. Diminished mEPSP amplitudes are observed in all conditions after PhTx application, while EPSP amplitudes are maintained at baseline levels due to a homeostatic increase in quantal content. **(B and C)** Quantification of EPSP amplitude (B) and normalized mEPSP amplitude and quantal content (C) in the indicated genotypes ($n \geq 7$; *t* test; Table S1). **(D)** Representative images of NMJ boutons immunostained with anti-BRP in the indicated genotypes at baseline and after PhTx application. **(E)** Quantification of mean intensity of BRP and vGlut puncta reveals a significant increase following PhTx application compared with baseline values (no PhTx). **(F)** An increase in the total fluorescence intensity of BRP and vGlut puncta per NMJ is observed in wild type, vGlut-OE, and *rab3* mutants after PhTx application ($n \geq 11$; *t* test; Table S1). Error bars indicate ± SEM. *, $P < 0.05$; **, $P < 0.01$; ***, $P < 0.001$; ****, $P < 0.0001$.

Table S2. **Key resources**

Reagent/resource	Source	Identifier
Antibodies		
Mouse anti-Synapsin (3C11)	DSHB	AB_2313867
Guinea pig anti-vGlut	Chen et al., 2017	N/A
Rabbit anti-Synaptotagmin 1	Mackler et al., 2002	N/A
Mouse anti-BRP (nc82)	DSHB	AB_2314866
Guinea pig anti-Unc13A	Böhme et al., 2016	N/A
Affinity-purified rabbit anti-GluRIII	Kiragasi et al., 2017	N/A
DyLight 405–conjugated secondary antibodies	Jackson ImmunoResearch	706-475-148, 715-475-150, 711-475-152
Alexa Fluor 488–conjugated secondary antibodies	Jackson ImmunoResearch	706-545-148, 715-545-150, 711-545-152
Alexa Fluor Cyanine 3–conjugated secondary antibodies	Jackson ImmunoResearch	706-165-148, 715-165-150, 711-165-152
Alexa Fluor 647–conjugated goat anti-HRP	Jackson ImmunoResearch	123-605-021
Goat anti-mouse Alexa Fluor 594	Thermo Fisher Scientific	A11032
Goat anti-guinea pig star635	Abberior	1-0101002
Experimental models: fly lines		
endo^{1}	Verstreken et al., 2002	N/A
endo$^{\Delta 4}$	Verstreken et al., 2002	N/A
GluRIIA^{sp16}	Petersen et al., 1997	N/A
elav^{c155}*-Gal4*	BDSC	BDSC #458
OK371-Gal4	Mahr and Aberle, 2006	N/A
OK6-Gal4	Aberle et al., 2002	N/A
UAS-vGlut	Daniels et al., 2004	N/A
rab3^{rup}	Graf et al., 2009	N/A
Cac$^{sfGFP\text{-}N}$	Gratz et al., 2019	N/A
UAS-arl8-GFP	Vukoja et al., 2018	N/A
arl8^{e00336}	Vukoja et al., 2018	N/A
UAS-endo RNAi (chromosome 3)	BDSC	BDSC #27679
UAS-Rab3 RNAi (chromosome 3)	BDSC	BDSC #31691
BRP-GFP	BDSC	BDSC #59292
vGlut-GFP	BDSC	BDSC #59411

N/A, not applicable.

Provided online is Table S1, showing absolute values for normalized data and additional statistics.

References

Aberle, H., A.P. Haghighi, R.D. Fetter, B.D. McCabe, T.R. Magalhães, and C.S. Goodman. 2002. wishful thinking encodes a BMP type II receptor that regulates synaptic growth in Drosophila. *Neuron.* 33:545–558. https://doi.org/10.1016/S0896-6273(02)00589-5

Böhme, M.A., C. Beis, S. Reddy-Alla, E. Reynolds, M.M. Mampell, A.T. Grasskamp, J. Lützkendorf, D.D. Bergeron, J.H. Driller, H. Babikir, et al. 2016. Active zone scaffolds differentially accumulate Unc13 isoforms to tune Ca(2+) channel-vesicle coupling. *Nat. Neurosci.* 19:1311–1320. https://doi.org/10.1038/nn.4364

Chen, X., W. Ma, S. Zhang, J. Paluch, W. Guo, and D.K. Dickman. 2017. The BLOC-1 Subunit Pallidin Facilitates Activity-Dependent Synaptic Vesicle Recycling. *eNeuro.* 4:1–18. https://doi.org/10.1523/ENEURO.0335-16.2017

Daniels, R.W., C.A. Collins, M.V. Gelfand, J. Dant, E.S. Brooks, D.E. Krantz, and A. DiAntonio. 2004. Increased expression of the Drosophila vesicular glutamate transporter leads to excess glutamate release and a compensatory decrease in quantal content. *J. Neurosci.* 24:10466–10474. https://doi.org/10.1523/JNEUROSCI.3001-04.2004

Graf, E.R., R.W. Daniels, R.W. Burgess, T.L. Schwarz, and A. DiAntonio. 2009. Rab3 dynamically controls protein composition at active zones. *Neuron.* 64: 663–677. https://doi.org/10.1016/j.neuron.2009.11.002

Gratz, S.J., P. Goel, J.J. Bruckner, R.X. Hernandez, K. Khateeb, G.T. Macleod, D. Dickman, and K.M. O'Connor-Giles. 2019. Endogenous tagging reveals differential regulation of Ca^{2+} channels at single AZs during presynaptic homeostatic potentiation and depression. *J. Neurosci.* 28:3068–3018.

Kiragasi, B., J. Wondolowski, Y. Li, and D.K. Dickman. 2017. A Presynaptic Glutamate Receptor Subunit Confers Robustness to Neurotransmission and Homeostatic Potentiation. *Cell Reports.* 19:2694–2706. https://doi.org/10.1016/j.celrep.2017.06.003

Mackler, J.M., J.A. Drummond, C.A. Loewen, I.M. Robinson, and N.E. Reist. 2002. The C(2)B Ca(2+)-binding motif of synaptotagmin is required for synaptic transmission in vivo. *Nature.* 418:340–344. https://doi.org/10.1038/nature00846

Mahr, A., and H. Aberle. 2006. The expression pattern of the Drosophila vesicular glutamate transporter: a marker protein for motoneurons and glutamatergic centers in the brain. *Gene Expr. Patterns.* 6:299–309. https://doi.org/10.1016/j.modgep.2005.07.006

Petersen, S.A., R.D. Fetter, J.N. Noordermeer, C.S. Goodman, and A. DiAntonio. 1997. Genetic analysis of glutamate receptors in Drosophila reveals a retrograde signal regulating presynaptic transmitter release. *Neuron.* 19:1237–1248. https://doi.org/10.1016/S0896-6273(00)80415-8

Verstreken, P., O. Kjaerulff, T.E. Lloyd, R. Atkinson, Y. Zhou, I.A. Meinertzhagen, and H.J. Bellen. 2002. Endophilin mutations block clathrin-mediated endocytosis but not neurotransmitter release. *Cell.* 109:101–112. https://doi.org/10.1016/S0092-8674(02)00688-8

Vukoja, A., U. Rey, A.G. Petzoldt, C. Ott, D. Vollweiter, C. Quentin, D. Puchkov, E. Reynolds, M. Lehmann, S. Hohensee, et al. 2018. Presynaptic Biogenesis Requires Axonal Transport of Lysosome-Related Vesicles. *Neuron.* 99:1216–1232.e7. https://doi.org/10.1016/j.neuron.2018.08.004